

# Fission of Nuclei far from Stability

K.-H. Schmidt<sup>a</sup>, J. Benlliure<sup>b</sup>, A. R. Junghans<sup>c</sup>

<sup>a</sup>Gesellschaft für Schwerionenforschung, Planckstraße 1, 64291 Darmstadt, Germany

<sup>b</sup>Universidad de Santiago de Compostela, 15706 Santiago de Compostela, Spain

<sup>c</sup>University of Washington, Center for Experimental Nuclear Physics and Astrophysics, Box 354290, Seattle WA 98195, U.S.A.

The secondary-beam facility of GSI provided the technical equipment for a new kind of fission experiment. Fission properties of short-lived neutron-deficient nuclei have been investigated in inverse kinematics. The measured element distributions reveal new kinds of systematics on shell structure and even-odd effects and lead to an improved understanding of structure effects in nuclear fission. The relevance of these studies for some presently considered applications is described. Prospects for future experiments are discussed.

*PACS:* 24.10.Pa; 24.30.Cz; 24.75.+i; 25.20.-x; 25.60.-t; 25.70.Mn; 25.85.Jg; 27.80.+w; 27.90.+b; 29.30.Aj

*Keywords:* Nuclear reactions; Radioactive beams; Nuclear fission; Measured fission-fragment elemental yields and total kinetic energies; Odd-even effect; Deduced fission channels; Applications of fission for incineration and secondary-beam production

## 1. INTRODUCTION

Nuclear fission is one of the most intensively studied types of nuclear reaction [1, 2], but still the experimental knowledge is rather incomplete. In the last three years, important progress has been achieved on this field by use of the new experimental facilities of GSI. In the present contribution, an overview on these new results is given.

Low-energy fission is a nuclear reaction at the extremes. But unlike many other studies, which try to reach the highest temperatures in nuclear systems, fission may start at zero temperature. It is a dramatic reordering of cold nuclear matter. It may start in the ground state as spontaneous fission and proceed by tunnelling through the fission barrier. Even when starting from excitation energies close to the fission barrier, the system has to pass through cold transition states at the barrier. Fission offers unique conditions to study the interplay of nuclear structure and dynamics, phenomena of nuclear structure at extreme deformation and the onset of dissipation in cold nuclei.

The fission process yields many observables. We will mainly concentrate on the fission-fragment distributions in  $Z$  and  $A$  and their kinetic energies. The understanding of the nuclide production in fission has acquired a renewed interest since its application for the production of neutron-rich secondary beams in next-generation secondary-beam facilities is intensively

discussed. This knowledge is also required for designing devices for the incineration of nuclear waste.

Fission-fragment distributions show two kinds of structure effects. One is caused by shell structure, the other one is related to the pairing correlations. When we consider that the additional binding energy due to shell and pairing effects amounts to a few per mill of the total binding energy of a heavy nucleus, these structure effects are strongly amplified in the fission process. In the following, we will shortly summarise the actual experimental situation and the present understanding of these pronounced structure effects in fission.

## 2. PREVIOUS KNOWLEDGE

All nuclei investigated from about  $^{229}\text{Th}$  to  $^{256}\text{Fm}$  were found to fission into fragments with strongly different mass. Symmetric fission is strongly suppressed. The mean mass of the heavy component is almost stationary. Obviously, shell effects in the heavy fragment control this asymmetric fission. The most important shells are considered to be the spherical  $N=82$  shell and a shell at  $N\approx 90$  at large deformation ( $\beta\approx 0.6$ ) [3].

But the asymmetric fission dies out on both extremes of the mass range. There is a dramatic change of the mass distribution to a narrow single-humped distribution found in  $^{258}\text{Fm}$  [4]. This is explained by the formation of two spherical nuclei close to the doubly magic  $^{132}\text{Sn}$ . Selected nuclei in this range are accessible to experiment because they decay by spontaneous fission. But also at the lower end one observes single-humped distributions, e.g. for  $^{213}\text{Ac}$ . However, these are much broader. A few mass distributions from low excitation energies could be measured by use of radioactive targets  $^{226}\text{Ra}$  and  $^{227}\text{Ac}$  (see e.g. [5]). Some nuclei in the suspected transition region between  $^{225}\text{Ac}$  and  $^{213}\text{At}$  have been produced with excitation energies around 30 MeV by fusion reactions [6, 7, 8].

In total, mass distributions have been measured for only 78 nuclei. Element distributions are a more direct signature of fission, because they are not modified by neutron evaporation from the excited fission fragments. They are measured with good resolution by in-flight methods for 9 fissioning nuclei only. Most of the research activity on nuclear fission has concentrated on a few nuclei, e.g. on  $^{235}\text{U}$  and  $^{239}\text{Pu}$ , to produce a tremendous amount of high-precision data necessary for the technical applications in nuclear reactors or in nuclear weapons. It is clear that, from a scientific point of view, the knowledge on nuclear fission is still rather scarce.

## 3. THE SECONDARY-BEAM EXPERIMENT

In a conventional fission experiment, a target nucleus is excited. The fission fragments reach the detectors with a kinetic energy given by the fission process. The available target materials limit the experiments on low-energy fission to a relatively small number of systems. Up to recently, spontaneous fission offered the only possibility to overcome this limitation for some very heavy nuclei which can be produced e.g. by heavy-ion fusion reactions.

The secondary-beam facility of GSI allows now becoming independent of available target nuclides. By fragmentation of a  $^{238}\text{U}$  beam at 1 A GeV, many short-lived radioactive nuclei are produced. After isotopic separation in the fragment separator, several hundred fissile nuclei are available for nuclear-fission studies [9,10,11].

The experiment consists of two parts. First, the secondary beam needs to be prepared and identified in mass and nuclear charge with the Fragment Separator FRS. Secondly, a dedicated set up is used to study fission in flight, i.e. in inverse kinematics. The whole experimental technique is described in detail in Ref. [12]. Fission is induced by Coulomb excitation of the secondary beam in the electromagnetic field of a high- $Z$  target nucleus. The energy-loss values and the velocity vectors of both fission fragments are measured, and the element distributions and the mean total kinetic energies are deduced.

### 3.1. Experimental setup

The experimental set up is shown in Fig. 1. It consists of a scintillator, the active secondary lead target, a subdivided double scintillator, a twin multi-sampling ionisation chamber (twin MUSIC), and a time-of-flight scintillator wall. The first scintillator provides position and time-of-flight information of the secondary beam. The active secondary target contains 5 lead foils with a total area density of  $3 \text{ g/cm}^2$  which make up a subdivided ionisation chamber. From the energy losses in the different sections, the foil in which fission occurred can be deduced, because the energy loss for two fission fragments is roughly only half the energy loss of the secondary projectiles before fission. With that information, fission originating from other layers of matter can efficiently be suppressed. The double scintillator acts as a fast trigger for fission events by requiring a coincidence of signals in the upper and lower detector. The twin MUSIC records the energy-loss signals of both fission fragments separately. In addition, it provides position information in vertical direction by means of the drift time of the electrons and in the horizontal direction by the pulse-height ratio of the diagonally subdivided anodes.

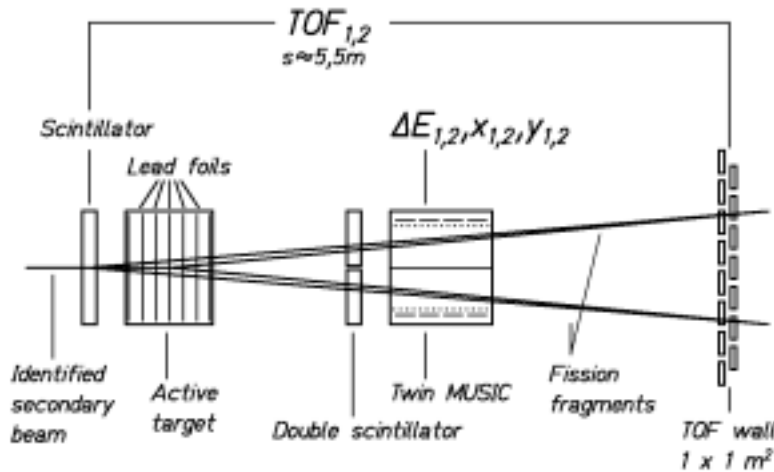


Fig. 1: Schematical drawing of the set up for the fission experiment with secondary beams.

The time of flight is measured by the first scintillator and the time-of-flight wall in order to determine the total kinetic energies and also to correct for the velocity dependence of the energy loss in the MUSIC to deduce the nuclear charges of the fission products.

In Fig. 2, the measured  $Z$ -response spectrum of fission fragments from electromagnetic-induced fission of  $^{226}\text{Th}$  is shown. Due to the high beam energy of typically 500 A MeV, all fission fragments are fully stripped, and a measurement of the energy loss allows to determine

the nuclear charge with high resolution. Furthermore they are emitted inside a narrow cone in forward direction with an opening angle of about 60 mrad with respect to the primary-beam direction. The detectors were designed to accept all fission fragments produced in the active target and the first scintillator. The detection efficiency amounted to 81%.

The success of a secondary-beam experiment relies on an efficient use of the limited beam intensity. Since two consecutive reactions are involved here, this is much more crucial than in a primary-beam experiment. In order to get a high ratio of detected secondary-reaction products to incoming primary projectiles, every link in the experimental chain needs to be optimised. In our fission experiment, this figure of merit amounted to  $3.2 \times 10^{-6}$ . Several conditions contribute to the efficient use of the available beam:

1. The magnitudes of the cross sections are all-important, as well for the production of the secondary beam as for the secondary reaction (i.e. fission after electromagnetic excitation).
2. The target area densities need to be very large.
3. High transport efficiencies of the secondary beam and the reaction products and high detection efficiency of the reaction products.
4. The large acceptance of the fragment separator which allowed to investigate 20 isotopes in one setting.

In all these points, the primary beam energy of 1 A GeV has a decisive influence: The cross section for electromagnetic excitation is strongly energy dependent, the usable target thickness depends directly on it, and it also ensures a high transport efficiency of the ions and allows to transmit 20 isotopes in one setting. The high beam energy is mandatory for the ion-optical separation of the heavy secondary projectiles, avoiding ambiguities and losses due to different ionic charge states that would occur at lower energies.

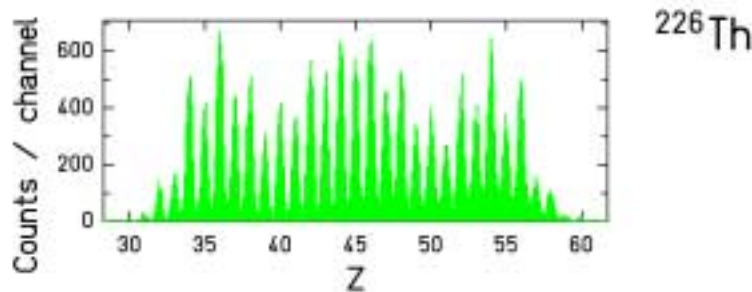


Fig. 2: Measured element distribution of the fission products of  $^{226}\text{Th}$  after electromagnetic excitation, deduced from the signals of the twin MUSIC.

### 3.2 Analysis

To extract fission-fragment element distributions after electromagnetic-induced fission, fission events originating from nuclear interactions with lead nuclei have to be suppressed. Fission in the first scintillator  $(\text{C}_9\text{H}_{10})_n$  is mainly induced by nuclear interactions, while in lead both electromagnetic excitations and nuclear reactions occur. Electromagnetic excitation preserves the number of protons in the secondary projectile, most nuclear reactions do not. With the good nuclear-charge resolution, see Fig. 2, we can reconstruct the charge of the fissioning nucleus by summing up the charges of the fission fragments.

By imposing the condition that the charge sum of the fission fragments equals the nuclear charge of the secondary projectiles, electromagnetic-induced fission can be highly enriched event-by-event. A small contribution from fission events, in which only neutrons were removed in the nuclear reaction can be subtracted if one assumes that it is identical to the appropriately weighted nuclear-charge spectrum originating from nuclear-induced fission in the scintillator, also accumulated under the condition that the sum of both fission-fragment charges equals the charge of the secondary projectiles. The details of this procedure are described in Ref. [12]. The condition on the charge-sum spectrum of the fission fragments also eliminates most events, which suffer from secondary reactions in the different layers of matter in the beam line. All events where the secondary beam loses protons upstream the secondary target are suppressed, and also reactions in which the fission fragments lose protons downstream the target are sorted out.

By summing up the counts in the peaks in the charge spectrum of the fission fragments after electromagnetic excitation measured by the twin MUSIC, the element distributions of the fission products could be determined. The total kinetic energy of the fission fragments was deduced from their velocity vectors, transformed into the centre-of-mass frame of the fissioning secondary projectile.

### 3.3 Excitation energies induced in the electromagnetic excitation

The electromagnetic field of a lead target nucleus as seen by the secondary projectiles can be formulated as a flux of equivalent photons according to Ref. [13]. At relativistic energies as employed here, the spectrum is hard enough to excite giant resonances in the secondary projectiles. With the calculated equivalent photon spectrum and the systematics of the photo-absorption cross sections, one can calculate the energy-differential cross section for electromagnetic excitation. This is one of the most important ingredients of the experiment, since it is important to have a sufficiently high excitation cross section to cope with the limited secondary-beam intensities. Although the excitation energy in every single event is not known precisely here, the excitation-energy distribution can be determined rather well on theoretical considerations, which are described in Ref. [12] and references therein.

The excitation-energy distributions of the investigated systems are all rather similar to each other in spite of the slight mass dependence of the resonance energies and the deformation-dependent splitting of the GDR. They peak at 11 MeV, and the high-energy part of the photo-absorption cross section is strongly suppressed, because the equivalent photon spectrum is steeply decreasing with energy. Therefore, the drastic variations of the structural effects found in the different systems as presented below cannot be explained by variations in the excitation-energy distribution. Excitations that exceed the fission barrier may lead to fission. However, also neutron evaporation has to be considered as the most important competing deexcitation channel. Its competition determines the fission probability as a function of energy, and it populates neighbouring nuclei at lower excitation energies which may also contribute to fission.

In the case of e.g.  $^{234}\text{U}$ , fission events induced by electromagnetic excitations are composed of about 80% first-chance fission ( $^{234}\text{U}$ ) 15% second-chance fission ( $^{233}\text{U}$ ) and a small fraction of higher-chance fission (mostly  $^{232}\text{U}$ ). The conditions for other secondary beams are expected to be similar. The measured fission probabilities always represent a mixture of about 3 isotopes, with first-chance fission dominating.

## 4. EXPERIMENTAL RESULTS

The data acquired in the secondary-beam experiment allow for the first time to systematically analyse the fission properties of nuclei in a continuously covered region on the chart of the nuclides. Figs. 3 and 4 show the elemental yields and the total kinetic energies after electromagnetic-induced fission, covering the transition from a single-humped element distribution at  $^{221}\text{Ac}$  to a double-humped element distribution at  $^{234}\text{U}$ . In the transitional region, around  $^{227}\text{Th}$ , triple-humped distributions appear, demonstrating comparable weights for asymmetric and symmetric fission.

An important parameter deduced from the data is the mean position of the heavy fission-fragment component shown in Fig. 5. From previously measured mass distributions, a roughly constant position of the heavy fission component in mass number had been deduced [14]. Due to the long isotopic chains investigated and the high precision of the data, we obtain a much more comprehensive view. It becomes very clear that the position of the heavy component is almost constant in atomic number  $Z \approx 54$  and moves considerably in neutron number. This also means that the position accordingly moves in mass number. It is not expected that any polarisation in  $N/Z$ , which is neglected here due to the UCD (unchanged charge density) assumption, can explain the variation of five units in neutron number. This is a surprising result, since the asymmetric fission component is usually traced back to the influence of neutron shells in the heavy component (e. g. [3]). This remarkable finding puts an important constraint on the theoretical understanding of the fission process. It may indicate that the shell effects in proton number play a more important role in asymmetric fission than thought previously.

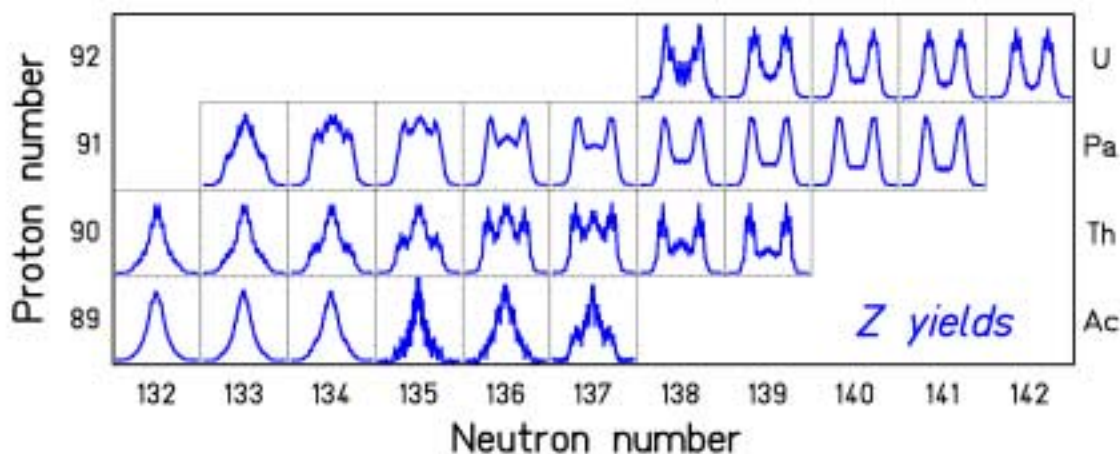


Fig. 3: Measured fission-fragment element distributions in the range  $Z = 24$  to  $Z = 65$  after electromagnetic excitation of 28 secondary beams between  $^{221}\text{Ac}$  and  $^{234}\text{U}$  are shown on a chart of the nuclides.

## 5. SIGNATURES OF SHELL EFFECTS IN FISSION

According to the present understanding of the fission process, the different components which appear in the yields and in the kinetic-energy distributions of the fission fragments are attributed to fission channels [15, 16, 17, 18] which are assigned to valleys in the potential-

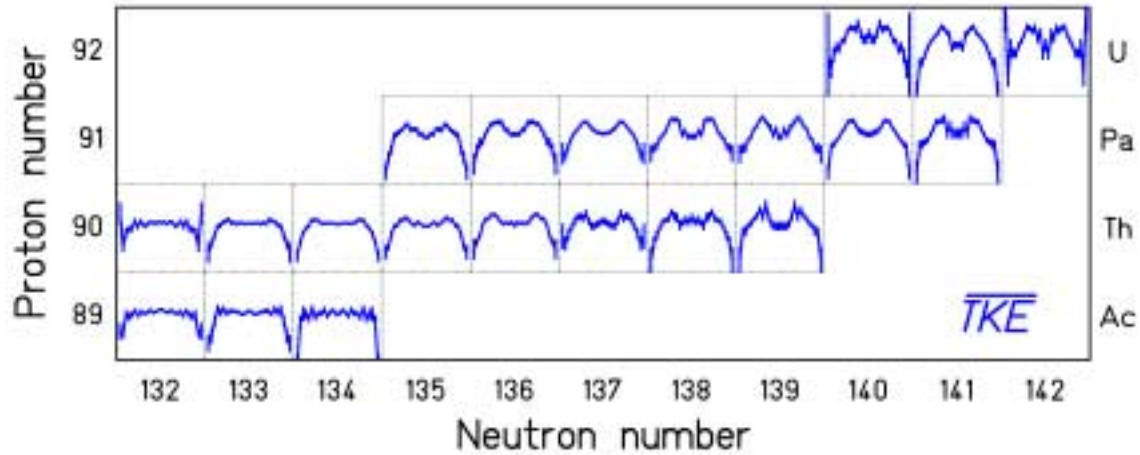


Fig. 4: Measured mean total kinetic energies as a function of the fission-fragment nuclear charge in the range  $Z = 31$  to  $Z = 59$  after electromagnetic excitation of 21 secondary beams between  $^{221}\text{Ac}$  and  $^{234}\text{U}$  are shown on a chart of the nuclides.

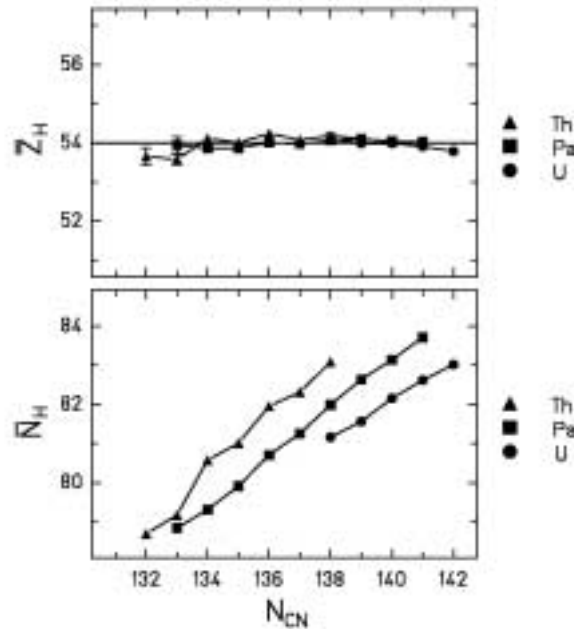


Fig. 5: Mean position of the heavy asymmetric component in nuclear-charge number  $Z_H$  (upper part) and neutron number  $N_H$  (lower part). While the charge number was measured, the neutron number was estimated by the UCD assumption:  $N_H = Z_H \times N_{CN} / Z_{CN}$ .

energy surface of the highly deformed system due to shell effects. Since it is not well understood, how the yields of the different fission channels are determined in the dynamic evolution of the fissioning system, it has become a standard to determine the parameters of the fission channels from a fit to the data by assuming that each of the independent fission channels is characterised by a Gaussian-like peak in the mass or element distribution and a specific elongation of the scission configuration which determines the total kinetic energy.

Fig. 6 shows the result of a fit to six selected systems, covering the transition from asymmetric fission to symmetric fission. Obviously, the measured data can well be represented by the superposition of three independent fission channels. A detailed comparison of the parameters of the fission channels determined here with those deduced previously for other fissioning systems goes beyond the scope of the present paper. We just mention that the systematic trends of the present data fit in rather nicely with the previous knowledge, except that the scission-point configuration of the “super-long” channel becomes more compact with decreasing mass number of the fissioning nucleus.

The theoretical work on structure effects in fission presently concentrates on the most realistic description of the shape-dependent potential-energy surface (e.g. Refs. [19, 20]). The results look complicated, and the minimisation with respect to higher-order shape distortions introduces hidden discontinuities. These discontinuities make it even more difficult to perform full dynamical calculations in order to obtain quantitative predictions of the isotopic distributions of fission fragments. Up to now, these calculations rather serve as a guide to qualitatively relate the structures in the data to those in the potential-energy landscape.

Since theory cannot yet provide us with a quantitative prediction, we tried to understand the data with a semi-empirical approach. The basic idea of our approach has been inspired by considerations of Itkis et al. [21]. We consider the fission barrier under the condition of a certain mass asymmetry. The height of the fission barrier  $V(A)$  is calculated as the sum of a liquid-drop barrier and two shells. The liquid-drop barrier is minimum at symmetry and grows quadratically as a function of mass asymmetry. The shell effects appear at  $N=82$  and  $N=90$ . A more detailed description of the model is given in Ref. [22]. This picture provides us with an explanation for the predominance of asymmetric fission of the actinides. In  $^{234}\text{U}$  like in most of the actinides, the lowest fission barrier appears for asymmetric mass splits. Approaching  $^{264}\text{Fm}$ , the shell effects at  $N=82$  in both fragments join, giving rise to a narrow symmetric mass distribution. In lighter nuclei, the influence of these shells on the fission process is weakened, because they add up to the higher liquid-drop potential at larger mass asymmetry. In  $^{208}\text{Pb}$ , the fission barrier is definitely lowest for symmetric mass splits.

A more quantitative description of this schematic model is given in Fig. 7. The mass yield  $Y(A)$  is assumed to be proportional to the phase space  $\rho(A)$  available above the fission barrier at a certain mass split. The initial excitation energy  $E^*$  above the mass-dependent barrier  $V(A)$  is available for intrinsic excitations. The shell effect in the level density is washed out with energy as proposed by Ignatyuk et al. [23]. The stiffness of the underlying liquid-drop potential is deduced from a systematics of the width of measured mass distributions [24]. The shells are modelled in a way that the calculated yields  $Y(Z)$  for  $^{227}\text{Th}$  are reproduced.

Now the model is applied to other nuclei ( $^{224}\text{Ac}$  and  $^{230}\text{Pa}$ ) without any further adjustment. The shells move up and down on the liquid-drop potential just a little bit due to the shift in neutron number of the fissioning nucleus. These tiny variations are sufficient to substantially modify the shape of the element distribution just as much as the experimental distributions change. This good reproduction of the data is a strong argument that this model gives the correct explanation for basic features of the transition from asymmetric to symmetric fission.

Figure 8 presents the element distributions, calculated with the same model, for all measured fissioning systems in comparison with the experimental data. There is an astonishingly good agreement with the experimental data for the whole systematics. This success of the very simple model might indicate that the dynamics of the fission process tends to wash out the influence of the details of the potential-energy landscape. It is to be expected that due to

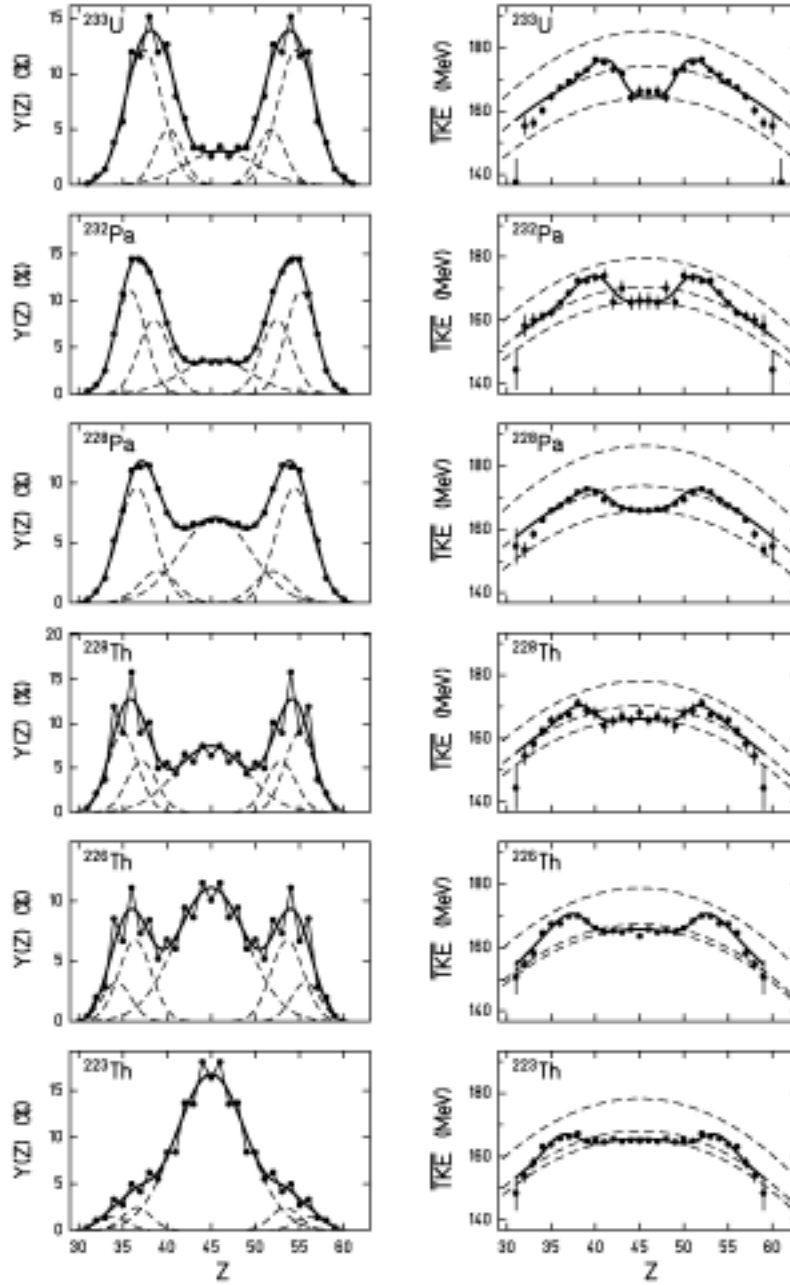


Fig. 6: Element yields (left part) and average total kinetic energies (right part) as a function of the nuclear charge measured for fission fragments of several fissioning nuclei after electromagnetic excitations. The data points are compared to the result of a simultaneous fit (full lines) with 3 fission channels. The yields are defined as the sum, and the total kinetic energies are defined as the mean value of the individual contributions of the different channels. The super-long, standard I and standard II channels correspond to the symmetric, the inner asymmetric and the outer asymmetric peaks (dashed lines), respectively, in the yields and to the lower, upper and middle curve (dashed lines), respectively, in the total kinetic energies.

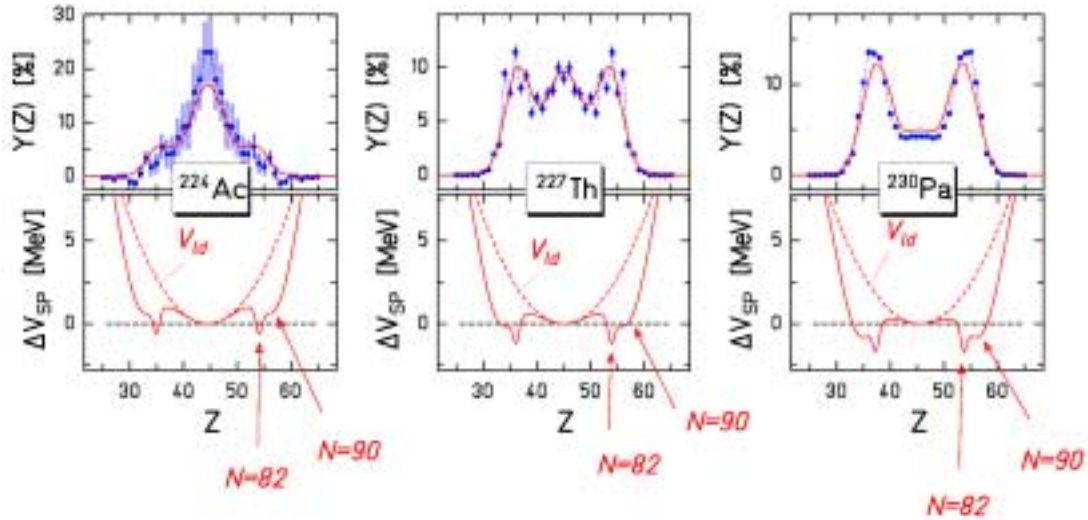


Fig.7: Measured element yields compared to the model predictions (upper parts), and the assumed variation  $\Delta V$  of the fission barrier as a function of the nuclear charge of one fission fragment with respect to the fission barrier for symmetric splits (lower parts).

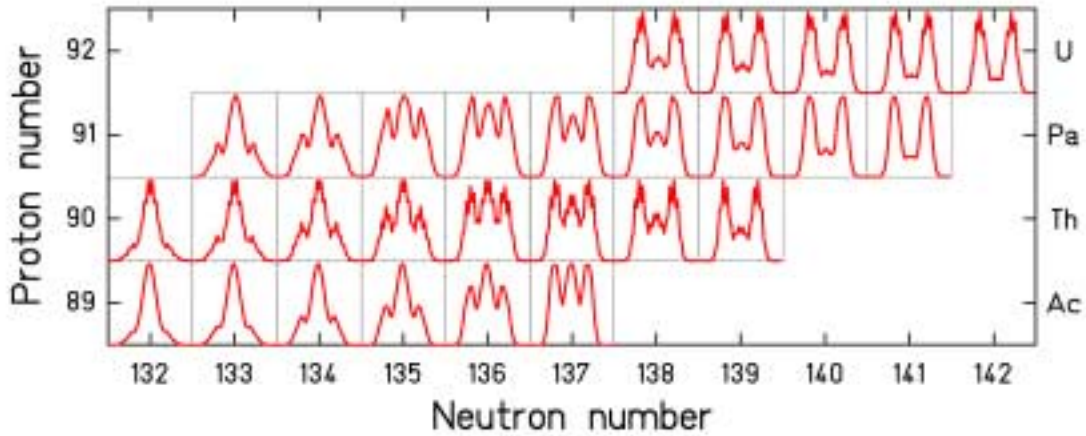


Fig. 8: Calculated element distributions of fission fragments from electromagnetic-induced fission of 28 systems from  $^{221}\text{Ac}$  to  $^{234}\text{U}$ .

the inertia of the collective motion the process does not feel every wiggle in the potential energy but rather takes a smooth trajectory.

## 6. SIGNATURES OF PAIRING CORRELATIONS IN NUCLEAR FISSION

Let us now address the even-odd structure found in the element distributions. From the large number of element distributions measured in our experiment, we could deduce a few new systematic trends. The first one is illustrated in Fig. 9. The left upper part shows the element distribution of  $^{220}\text{Ac}$ . It looks smooth at the first sight. But an expanded view on the

wings of the distribution reveals a strong even-odd structure. With respect to a smooth distribution, there is an enhanced production of even- $Z$  elements in the light tail and an enhanced production of odd- $Z$  elements in the heavy tail. The local even-odd structure can quantitatively be determined by the logarithmic third difference  $\delta_Z$ , introduced by Tracy et al. [25]. The local even-odd effect amounts to more than 20% in the wings. The same effect is found for  $^{228}\text{Pa}$ . Also all the other odd- $Z$  fissioning systems investigated show the same feature. We conclude that the unpaired proton prefers to go to the heavy fragment which offers a larger phase space for excited unpaired nucleons due to the larger single-particle level density. This is an indication for the validity of the statistical model in describing the fission-fragment even-odd structure.

The secondary-beam experiment is the first one to yield the even-odd effect for symmetric charge splits. This allows following the variation of the even-odd effect in even- $Z$  fissioning systems over a large range of charge asymmetry, from symmetry to extreme asymmetry. We observe a strong increase of the local even-odd effect in the wings of the distribution as can be seen in Fig. 10 for  $^{226}\text{Th}$  and  $^{223}\text{U}$ . Also all the other even- $Z$  fissioning systems show the same feature. We explain this finding again by the larger single-particle level density in the heavier fragment. When one proton pair is broken, the unpaired protons both prefer the heavy fragment. Previously, an increased local even-odd effect in extremely asymmetric fission found in  $^{235}\text{U}(\text{n}_{\text{th}},\text{f})$  was interpreted as a direct measure of the temperature at scission [26]. This interpretation must be revised on the basis of our new results [27].

These new features found in the even-odd structures of fission-fragment distributions [27], which are not explained by any of the available models [28,29], motivated us to reconsider the theoretical understanding of pair breaking in fission [30]. These considerations allowed us to address a long-standing puzzle, the different magnitudes of even-odd structures in neutron and proton number. Fission-fragment distributions measured at very high total kinetic energies allow determining primary yields in proton and neutron number, since neutron evaporation is impossible or strongly suppressed. Data of this nature only exist for a few systems,  $^{233}\text{U}(\text{n}_{\text{th}},\text{f})$ ,  $^{235}\text{U}(\text{n}_{\text{th}},\text{f})$ ,  $^{239}\text{Pu}(\text{n}_{\text{th}},\text{f})$ , and spontaneous fission of  $^{252}\text{Cf}$  [31,32,33,34,35,36]. The even-odd effect in proton number is found to be much larger than the even-odd effect in neutron number, although the even-odd structures in proton and neutron number in the binding energies are about equal.

In the new model, the nucleus is considered as a two-component super-fluid system. If the dissipation process from saddle to scission leads to quasi-particle excitations, still one of the subsystems may remain completely paired. We formulated the probability  $P_0^Z$  to preserve a completely paired proton configuration as the probability to store all the dissipated energy in the neutron subsystem. It is given by the partial level density of pure neutron excitations divided by the total level density. The probability  $P_0^N$  to preserve a completely paired neutron configuration can be calculated in an analogous way by the partial level density of pure proton excitations divided by the total level density. Independently of the excitation mechanism, we assume that the quasi-particle excitations of protons and neutrons are in thermal equilibrium.

The special feature of the new model is the rigorous formulation of the density of quasi-particle excitations on the basis of the super-fluid nuclear model in a micro-canonical approach. It is important to consider the competition between neutron- and proton-quasi-particle excitations in the two-component nuclear system for the well-defined energy available. Statistical-model considerations (e.g. by Fong [37]) or thermo-dynamical approaches (e.g. by Wilkins et al. [3] or Manzouranis and Nix [29]) based on the macro-canonical approach lead to fundamentally different predictions.

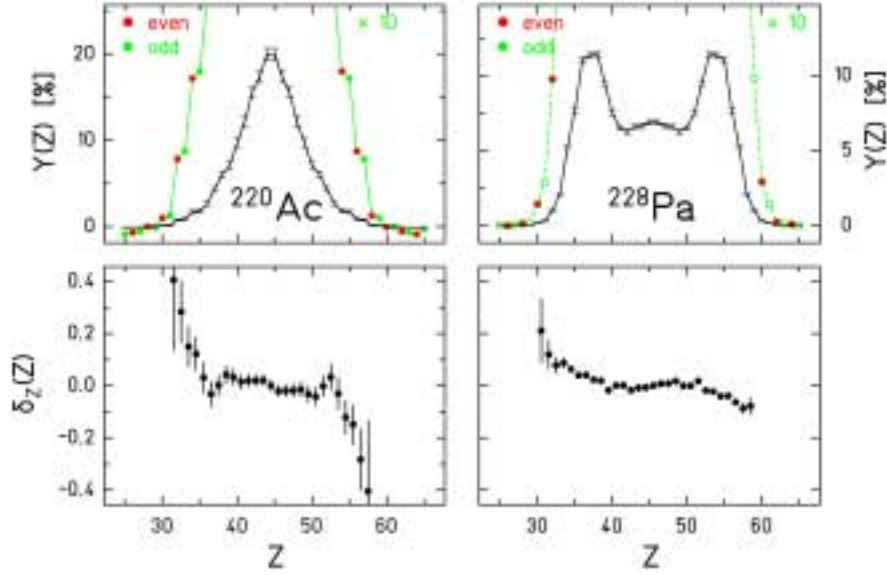


Fig. 9: Measured element distributions (upper part) and deduced local even-odd effect (lower part) after electromagnetic fission of  $^{220}\text{Ac}$  and  $^{228}\text{Pa}$ .

The result of the model is shown in Fig. 11. Due to the neutron excess in the fissioning nuclei,  $P_0^Z$  is much larger than  $P_0^N$ . In contrast to previously proposed models, this difference is obtained naturally without any adjustable parameter.

It is not so obvious, in which way our predictions can be compared to the available experimental results, since the intrinsic excitation energy at scission cannot be measured. Only data at very high fission-fragment kinetic energies are suited, where neutron evaporation is inhibited. The difference of the measured total kinetic energy (TKE) of the fragments from the  $Q$  values, denoted as total excitation energy (TXE), which is used as an ordering parameter in refs. [35,36,38] is certainly not a good measure for the excitation energy at scission, because this value fluctuates strongly with the partition of nucleons for similar pre-scission configurations. Tentatively, we compare the predicted  $P_0^N$  and  $P_0^Z$  values with the even-odd effect observed at constant TXE, averaged over the even-odd structure as discussed in ref. [31]. In some approximation, a constant averaged TXE corresponds to a constant kinetic energy of the light fission fragment (see e.g. [34]). (We assume here that there is no direct coupling between pre-scission kinetic energy and pair breaking.)

When the measured even-odd effects in proton number of  $^{233}\text{U}(\text{n}_{\text{th}},\text{f})$ ,  $^{235}\text{U}(\text{n}_{\text{th}},\text{f})$ , and  $^{239}\text{Pu}(\text{n}_{\text{th}},\text{f})$ , are taken to determine the excitation energy at scission, the resulting even-odd effects in neutron number coincide rather well with the theoretical curve. Also for the spontaneous fission of  $^{252}\text{Cf}$ , the even-odd structure in proton number is much stronger than that in neutron number, although the even-odd effect in neutron number is even smaller than expected by the model. Comparing our model with the measured proton even-odd effect, the TXE values between 7 and 15 MeV correspond to excitation energies at scission between 5 and 7 MeV. The difference could be attributed to deformation energy at scission which decreases at high TKE as expected due to the more compact scission configuration. A compari-

son with data of other systems which are given as a function of TXE of the specific splits [35,36] is beyond the scope of this paper. We conclude that the large difference found in the even-odd structure in proton and neutron number finds at least its qualitative explanation in the frame of the statistical model, provided the available phase space is rigorously calculated.

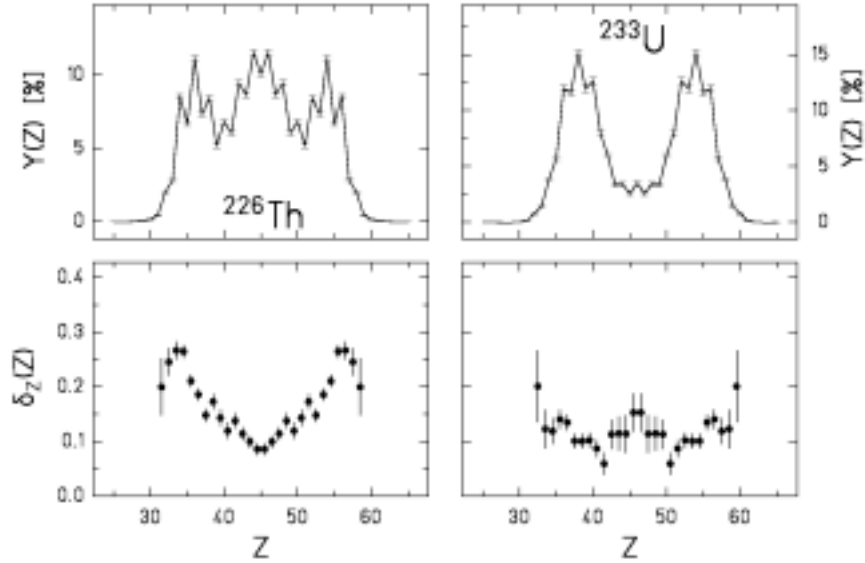


Fig. 10: Measured element distributions (upper part) and deduced local even-odd effect (lower part) after electromagnetic fission of  $^{226}\text{Th}$  and  $^{233}\text{U}$ .

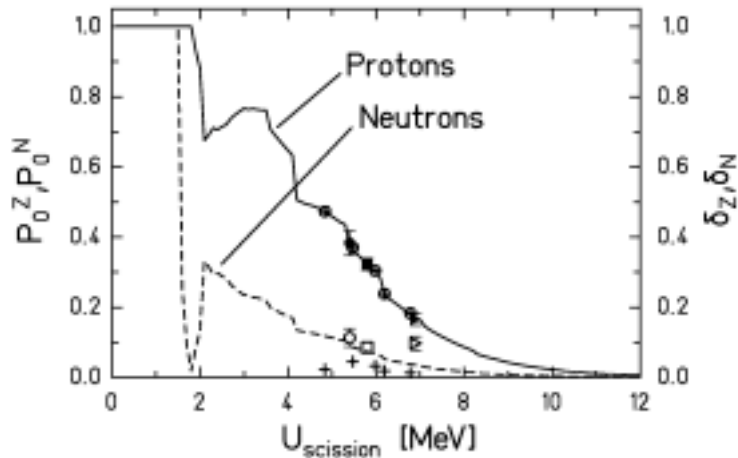


Fig. 11: Calculated survival probabilities of the completely paired proton and neutron configurations as a function of excitation energy at scission (left scale) and experimental data on the proton (full symbols) and neutron (open symbols) global even-odd effects at high kinetic energies of the light fragments (right scale) for the fissioning nuclei  $^{234}\text{U}$  ( $E_{\text{kin}} = 111$  MeV) [31] as circles,  $^{236}\text{U}$  ( $E_{\text{kin}}=108$  MeV) [32] as squares, and  $^{240}\text{Pu}$  ( $E_{\text{kin}} = 111$  MeV) [33] as triangles. In addition, the global even-odd effects for protons ( $\oplus$ ) and neutrons ( $+$ ) at bins of constant TXE (around 7, 9, 11, 13 and 15 MeV) are shown for spontaneous fission of  $^{252}\text{Cf}$  [34].

## 7. APPLICATIONS

Recently, two fields for the application of nuclear fission have attracted much interest: the production of medium-mass neutron-rich nuclides for fundamental research and the incineration of minor actinides produced in nuclear reactors. Both applications require a precise knowledge of the properties of the residues produced in the fission of non-stable heavy nuclei. The experimental technique and the results presented in this work are highly relevant for those investigations.

### 7.1 Production of medium-mass neutron-rich nuclides

Fission is a widely used process to produce neutron-rich nuclei by irradiating a fissile target, with neutrons from a neutron source or with high-energy protons in an ISOL system. In an ISOL system the neutron-rich nuclei have to be extracted out of the target and re-ionised, which relies on the chemical volatility of the elements in question and restricts the accessible range in atomic number and half-life. In low-energy neutron-induced fission, the distribution of neutron-rich nuclei is given by the distribution of fission fragments of the compound nucleus after neutron capture. Fission of relativistic  $^{238}\text{U}$  projectiles in a beryllium target [39] has proven to be very useful in the production of exotic nuclei, e.g. the doubly magic  $^{78}\text{Ni}$  was produced using this technique. As this is fission in flight, there is no dependence on the chemical properties of the elements involved, and the separation time is smaller than  $10^{-6}$  seconds, so even very short-lived isotopes can be studied.

Fission and fragmentation of a relativistic  $^{238}\text{U}$  beam is a complex reaction, where not only the projectile nucleus may undergo fission, but also a distribution of highly-excited intermediate prefragments. Thus, the resulting distribution of fission fragments is substantially different from low-energy fission of a single nucleus. The nuclei contributing to fission are just the nuclei whose properties have been studied in our secondary-beam experiment. The semi-empirical fission model of Ref. [22] discussed in section 5.2 is very well suited to describe the fission properties of these nuclei and can therefore be used to make realistic predictions for the production cross sections of exotic nuclei, which are key quantities in the design of the next generation exotic-beam facilities. The fission model has been used together with the Abrasion-Ablation Model ABRABLA, Ref.[40, 41], to describe projectile fragmentation of heavy, fissile nuclei.

Fission and fragmentation of  $^{238}\text{U}$  in a lead target has been studied in great detail [42] between vanadium ( $Z=23$ ) and rhenium ( $Z=75$ ). There, both fission after electromagnetic excitation and nuclear-induced fission are preeminent. More than 600 nuclide cross sections for fragmentation and for fission have been measured. These data show the characteristics of the reactions contributing to the production of exotic nuclei:

1. Electromagnetic-induced fission, which is mainly fission of the projectile nucleus at low excitation energy around 11 MeV.
2. Nuclear-induced fission of neutron-deficient actinides lighter than  $^{238}\text{U}$ . The excitation-energy range of fission is rather broad, and the number of fissioning nuclei is large.
3. Deexcitation of the projectile prefragments by evaporation of neutrons and charged particles. The residues populate an extended range due to the large fluctuations in excitation energy and  $N/Z$  ratio. The main production lies on the neutron-deficient side of  $\beta$  stability.

Neutron-rich heavy nuclei can be produced in a special class of reactions, the cold-fragmentation reaction. At the extreme, the projectile may lose only protons without intro-

ducing excitation energies above the neutron separation energy. Up to now, the 5-proton removal channel could be observed in the reaction  $^{197}\text{Au}$  (950 A MeV) + Be [43].

The upper part of Fig. 12 contains the measured production cross sections on a chart of the nuclides. One can clearly see the double-humped structure of the light and heavy fission fragments from electromagnetic-induced fission of  $^{238}\text{U}$  and the corridor of evaporation residues on the left side of the stable nuclides. In addition, fission from higher excitation energies leads to nuclei close to  $\beta$  stability. By measuring the velocity distribution, fragments from fission and fragmentation can be separated kinematically, see Ref. [42].

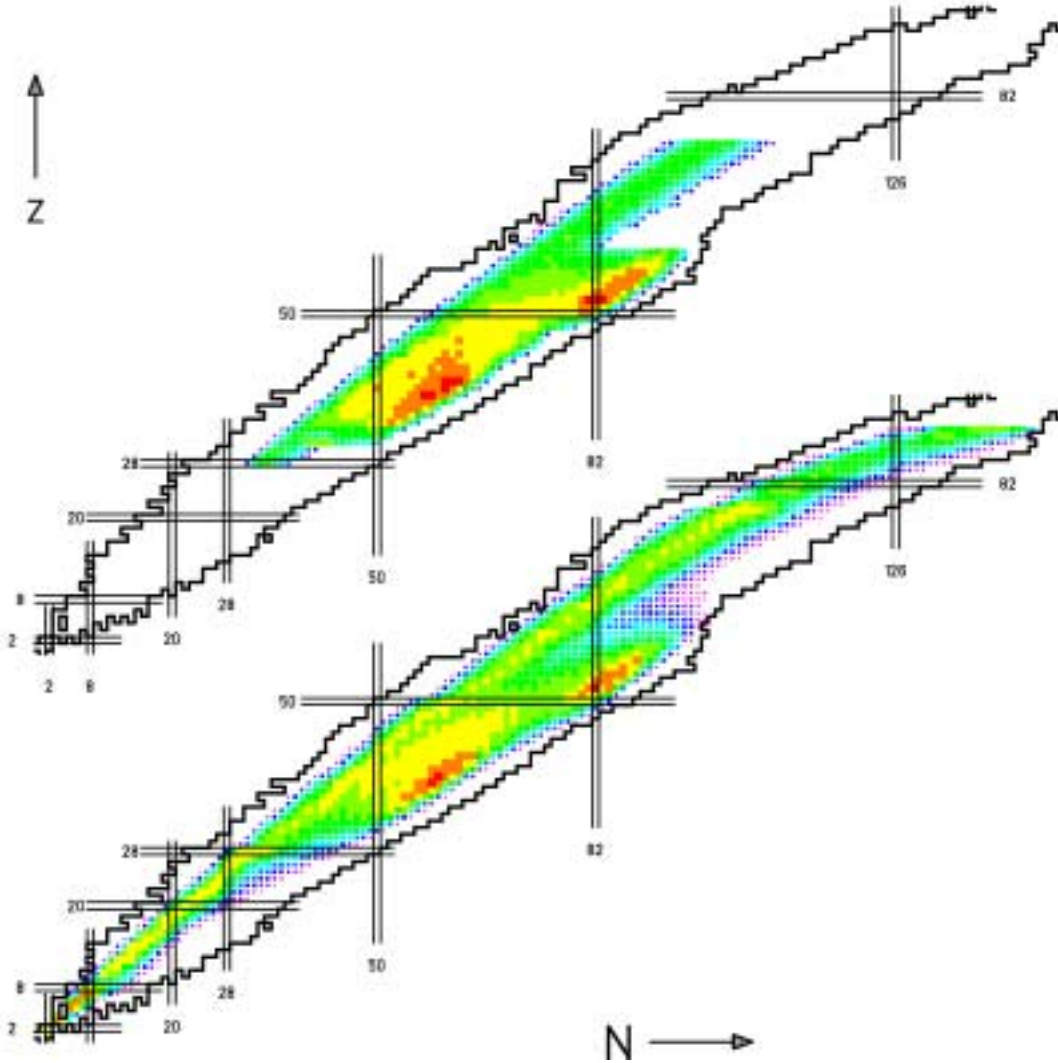


Fig. 12. Measured [42] (upper part) and calculated [22] (lower part) nuclide distribution, produced in the reaction  $^{238}\text{U}$  (1 A GeV) +  $^{208}\text{Pb}$  in the range from 0.01 mb to 100 mb.

The lower part shows the calculated yields on the same scale using ABRABLA including the fission model. The simulation extends to lower cross sections than the experiment. In general, the agreement between data and calculation is better than a factor of 2, therefore it is

possible to estimate production rates for future facilities with these calculations. An overview on the nuclide production in other systems measured in inverse kinematics and some general considerations on the production of secondary beams can be found in Refs. [44, 45]. The choice of the optimal production method and the target and projectile combination is not trivial and depends on the detailed understanding of the contributing processes. The calculated production cross sections together with the parameters of the experiment, accelerator and spectrometer are the basis for realistic estimations.

The present experiments also provide valuable information on the production of neutron-rich isotopes in fission reactions of heavy non-stable nuclei. The fission reactions of heavy actinides like  $^{234}\text{Am}$  or  $^{244}\text{Cm}$  would lead to the production of more neutron-rich isotopes than the ones produced with  $^{238}\text{U}$ . In contrast, in these heavier systems, the shell effects governing the asymmetric mass distribution of fission residues would reduce the production of neutron-rich isotopes of lighter elements.

The production rates of neutron-rich isotopes obtained with these reactions could be evaluated by extrapolating the knowledge acquired from the investigations presented in this work. The direct measurement of the production yields in these reactions using heavier projectiles represents a more ambitious option.

## 7.2 Incineration of minor actinides

A second domain of application of these experiments is related with the incineration of minor actinides produced in nuclear reactors or stored in nuclear weapons. Recently, it was proposed to partially transmute these radioactive residues by using subcritical devices fed with a spallation neutron source [46]. The reliability of such devices relies on a precise knowledge of the nuclear reactions involved in its operation.

Although the incineration process of actinides is governed by the neutron-capture and fission cross sections, the knowledge on mass and charge distributions of the fission residues induced by fast neutrons on actinides is needed, too. These distributions will determine the production rates of secondary long-lived fission residues. Some of the systems to be investigated are:  $^{234}\text{U}$ ,  $^{236}\text{U}$ ,  $^{237}\text{Np}$ ,  $^{238}\text{Pu}$ ,  $^{241}\text{Am}$ ,  $^{242\text{m}}\text{Am}$ ,  $^{243}\text{Am}$ ,  $^{242}\text{Cm}$ ,  $^{243}\text{Cm}$ ,  $^{244}\text{Cm}$ . Together with the incineration of minor actinides, it has also been proposed to use the thorium-cycle for energy production [47]. The radioactive inventory produced with this fuel will depend on the characteristics of the residues produced in the fission of thorium and protactinium isotopes.

Once more, the knowledge acquired in the fission experiments with secondary beams can be used directly for the thorium cycle or extrapolated to investigate the incineration of minor actinides. In fact, this experiment allowed to validate the model calculations presented in section 5.2. These calculations can be applied to describe the mass and charge distributions of residues produced in fast-neutron-induced fission reactions. In Fig. 13, we compare some mass distributions of residues produced in fission reactions induced by fast neutrons and protons. The calculated distributions provide a good description of the measured data.

It would be even more interesting to measure the mass and charge distributions of the residues produced in these reactions directly. Unfortunately, when we compare with our present experiments, two main difficulties should be overcome: the production of actinides to be investigated at relativistic energies and a better determination of the excitation energy. The first difficulty can be overcome partially by using charge pickup or charge exchange reactions of  $^{238}\text{U}$  at relativistic energies [48]. These reactions would allow to investigate the fission proc-

ess in some neptunium isotopes with the present technique. A better determination of the excitation energy would require an improved experimental technique as considered below.

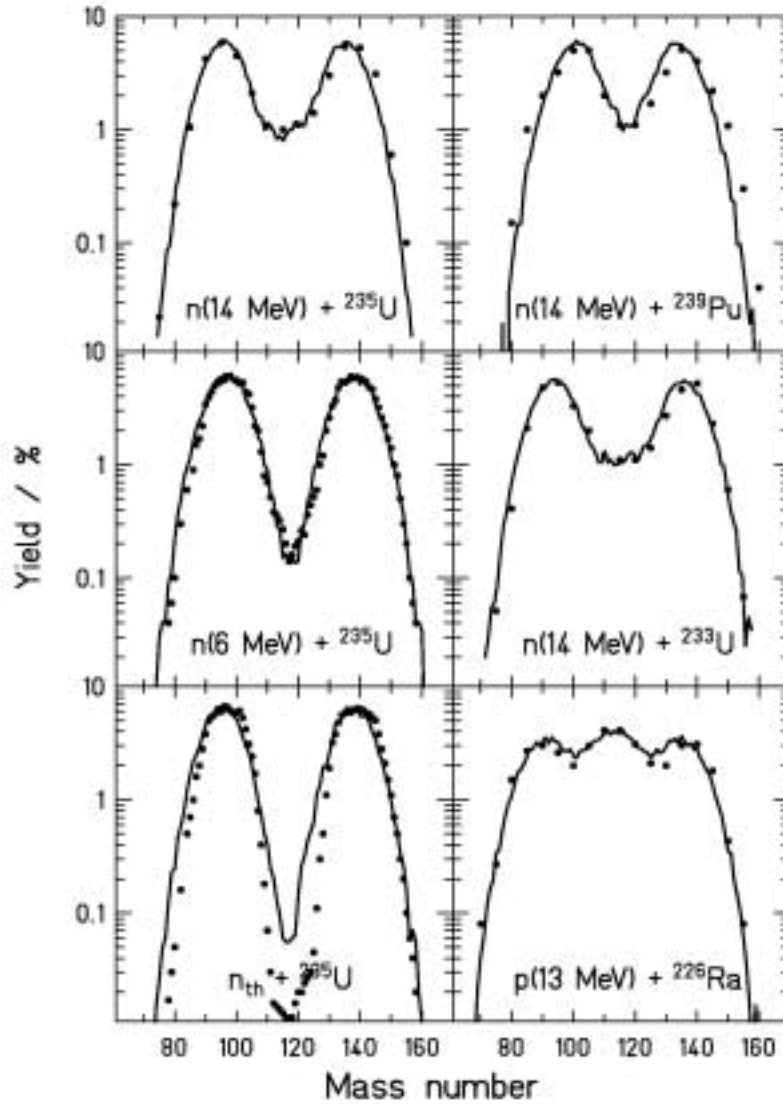


Figure 13: Mass distributions of residues produced in fission reactions induced by fast neutrons and protons. The data, refs. [49,50,51,52], are compared with the model calculations described in section 5.2.

## 8. FUTURE TRENDS FOR FISSION EXPERIMENTS WITH SECONDARY BEAMS

In spite of the success of the experiment presented in this paper, several improvements are conceivable in the future. We will first present a scenario which seems to be in reach by combining elaborate experimental equipment which has already been used in other experiments. The second, even more ambitious scenario will require important new installations.

The experimental technique employed so far for the fission studies did allow to measure the element distribution of the fission fragments and their velocities, by measuring the energy loss in an ionisation chamber and the time of flight of the fission fragments. The logical continuation of the experimental method is to perform an experiment which is approaching kinematical completeness by measuring the mass of the fission fragments the multiplicity of the neutrons evaporated and the sum-energy of the emitted gamma-rays. This requires a magnetic dipole spectrometer set up with a large-area neutron detector (LAND) and a detector system for determining the velocity of the fission fragments, e.g. a Cerenkov counter. The required resolution in magnetic rigidity is  $B\rho/\Delta B\rho = 300$ . Figure 14 shows a scenario at GSI, that still contains quite some experimental challenges, which cannot be discussed here in detail. The new aspects of fission accessible with this kind of setup are, that now one can study the influence of protons and neutrons separately. By knowing the excitation energy of the final products one can get a hold on the temperature dependence of fission dynamics.

Compared to the previous experiments performed directly behind the FRS, the additional knowledge of the mass number of the fission fragments better defines the influence of shell structure in both neutron and proton number, in particular in charge polarisation. Also, the studies on fluctuations in the charge polarisation, interpreted as an interplay of quantum oscillations and collective motion, can be extended to lighter fissioning systems. New results on the dynamic evolution of the fissioning system from saddle to scission are expected in a particularly interesting region of multimodal fission.

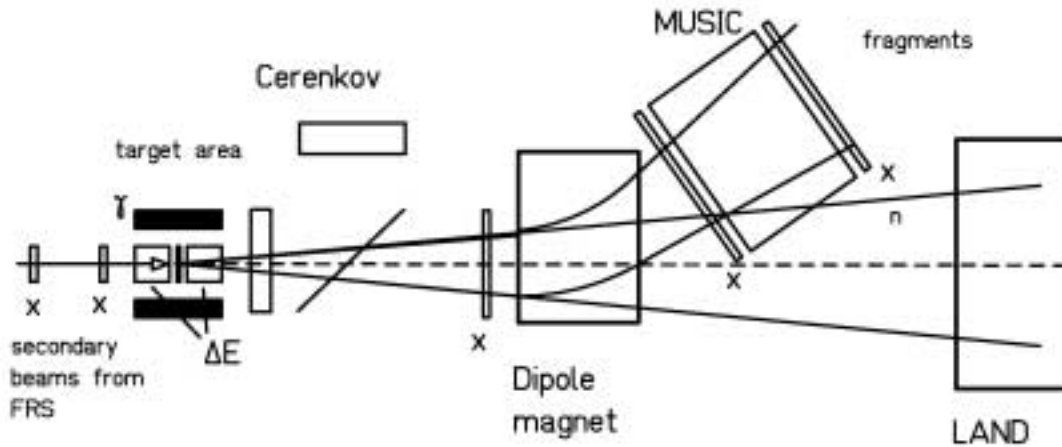


Fig. 14: Schematic drawing of a next-generation fission experiment with secondary beams.

The use of high-energetic secondary beams for the fission experiments requires the use of inverse-kinematic techniques. This brings along a number of advantages. Probably the most important one is the excellent  $Z$  resolution achieved. However, the electromagnetic excitation which has been chosen due to its large cross section induces a rather broad excitation-energy distribution. Therefore, one is interested to apply a more specific excitation mechanism. A possible solution of this problem could be provided by an electron-ion collider where the secondary projectiles are excited by inelastic electron scattering [53]. However, the complexity of such an experimental set up will be enormous. In particular the construction of an adapted

electron spectrometer will be a difficult task. Very high beam intensities will be required in order to reach the necessary luminosity.

## 9. SUMMARY

Nuclear fission is a unique laboratory for studying the dynamical properties of cold nuclei. There are two essential very specific features which are not found in other systems. Firstly, the electric charge in nuclei is homogeneously distributed over the whole volume. This gives rise to a “true” fission process which is essentially symmetric. Shell effects modulate this feature. Secondly, cold nuclei are two-component superfluid systems. This gives rise to particularly complex features in pair breaking which are not yet fully explored.

Experiments with secondary beams using elaborate experimental installations available at GSI opened up new possibilities for experimental studies of nuclear fission. Element yields and total kinetic energies have been determined for 70 fissioning systems from  $^{205}\text{At}$  to  $^{234}\text{U}$ . This way, new systematic results for a continuous region of fissioning systems have been obtained. The new results are consistent with statistical concepts to an astonishingly high degree. This also holds for even-odd structures in neutrons and protons if the quasi-particle excitations are properly calculated. Although the full understanding of the dynamics of fission is still missing, one came closer to a quantitative description of structure effects in fission.

Besides the scientific interest in a better understanding of the influence of nuclear structure on a large-amplitude collective motion, several applications like the production of neutron-rich secondary projectiles in next-generation secondary-beam facilities and the design of devices for the incineration of nuclear waste profit from the better experimental knowledge on nuclear fission brought about by the fission experiments with secondary beams.

In the future, the use of more elaborate experimental equipment which is even better adapted to the specific conditions of inverse kinematics will allow to obtain kinematically more complete information about the nuclear-fission process for nuclei far from stability.

## ACKNOWLEDGEMENT

This work comprises the results of a dedicated research program on nuclear fission, performed at GSI Darmstadt as documented in the references given. In particular, we would like to mention the contributions of P. Armbruster, C. Böckstiegel, H.-G. Clerc, T. Enqvist, A. Grewe, A. Heinz, A. V. Ignatyuk, M. deJong, F. Rejmund, and S. Steinhäuser.

## REFERENCES

1. R. Vandenbosch, J. R. Huizenga, Nuclear Fission (New York: Academic), 1973.
2. The Nuclear Fission Process, C. Wagemans, ed., CRC Press, London, 1991.
3. B. D. Wilkins, E. P. Steinberg, R. R. Chasman, Phys. Rev. **C 14** (1976) 1832.
4. D. C. Hoffman, M. R. Lane, Radiochimica Acta **70/71** (1995) 135.
5. H. J. Specht, Phys. Scripta **10 A** (1974) 21.
6. I. Nishinaka et al., Phys. Rev. **C 56** (1997) 891.
7. I. V. Pokrovsky et al., Phys. Rev. **C 60** (1999) 041304.

- 
8. I. V. Pokrovsky et al., Phys. Rev. **C 62** (2000) 014615.
  9. K.-H. Schmidt et al., Phys. Lett. **B 325** (1994) 313.
  10. H.-G. Clerc et al., Nucl. Phys. **A 590** (1995) 785.
  11. A. R. Junghans et al., Nucl. Phys. **A 629** (1998) 635.
  12. K.-H. Schmidt et al., Nucl. Phys. **A 665** (2000) 221.
  13. G. Baur, C. A. Bertulani, Phys. Rev. **C 34** (1986) 1654.
  14. K. F. Flynn et al., Phys. Rev. **C 5** (1972) 1725.
  15. A. Turkevich, J. B. Niday, Phys. Rev. **84** (1951) 52.
  16. V. V. Pashkevich, Nucl. Phys. **A 169** (1971) 275.
  17. M. G. Mustafa, U. Mosel, H. W. Schmitt, Phys. Rev. **C 7** (1973) 1519.
  18. U. Brosa, S. Grossmann, A. Müller, Phys. Rep. **197** (1990) 167.
  19. V. V. Pashkevich, Nucl. Phys. **A 477** (1988) 1.
  20. P. Möller, A. Iwamoto, Phys. Rev. **C 61** (2000) 047602.
  21. M. G. Itkis et al., Sov. J. Part. Nucl. **19** (1988) 301.
  22. J. Benlliure et al., Nucl. Phys. **A 628** (1998) 458.
  23. A. V. Ignatyuk et al., Yad. Fiz. **21** (1975) 485 (Sov. J. Nucl. Phys. **21** (1975) 255).
  24. S. I. Mulgin et al., Nucl. Phys. **A 640** (1998) 375.
  25. B. L. Tracy et al., Phys. Rev. **C 5** (1972) 222.
  26. J. L. Sida et al., Nucl. Phys. **A 502** (1989) 233c.
  27. S. Steinhäuser et al., Nucl. Phys. **A 634** (1998) 89.
  28. H. Nifenecker et al., Z. Phys **A 308** (1982) 39.
  29. G. Mantzouranis, J. R. Nix, Phys. Rev. **C 25** (1982) 918.
  30. F. Rejmund et al., Nucl. Phys. **A 678** (2000) 215.
  31. U. Quade et al., Nucl. Phys. **A 487** (1988) 1.
  32. W. Lang et al., Nucl. Phys. **A 345** (1980) 34.
  33. C. Schmitt et al., Nucl. Phys. **A 430** (1984) 21.
  34. H.-H. Knitter et al., Nucl. Phys. **A536** (1992) 221.
  35. J. Trochon et al., Proc. Int. Conf. 50 years nucl. fission, Gaithersburg, USA, 1989, p. 313.
  36. W. Schwab et al., Nucl. Phys. **A 577** (1994) 674.
  37. P. Fong, Phys. Rev. **102** (1956) 434.
  38. F.-J. Hamsch et al., Nucl. Phys. **A 554** (1993) 209.
  39. Ch. Engelmann et al., Z. Phys. **A 352** (1995) 351.
  40. J.-J. Gaimard, K.-H. Schmidt, Nucl. Phys. **A 531** (1991) 709.
  41. A. V. Ignatyuk et al., Nucl. Phys. **A 593** (1995) 519.
  42. T. Enqvist et al., Nucl. Phys. **A 658** (1999) 47.
  43. J. Benlliure et al., Nucl. Phys. **A 660** (1999) 87.
  44. J. Benlliure et al., Proc. XXXVII Int. W. Meeting on Nucl. Phys., Bormio (Italy), 1999.
  45. K.-H. Schmidt et al., Proc. 5th Int. Conf. Rad. Nucl. Beams, Divonne (France), 2000.
  46. C. D. Bowman et al., Nucl. Instr. and Methods **A 320** (1992) 336.
  47. C. Rubbia et al., CERN report 1995, CERN/AT/95-44(ET).
  48. Th. Rubehn et al., Phys. Rev. **C 53** (1996) 993.
  49. Ch. Straede et al., Nucl. Phys. **A 462** (1987) 129.
  50. D. G. Perry, A. W. Fairhall, Phys. Rev. **C 4** (1971) 977.
  51. E. A. C. Crouch, At. Nucl. Data Tab. **19** (1977) 418.
  52. J. E. Gindler et al., Phys. Rev. **C 27** (1983) 2058.
  53. Th. Weber et al., Nucl. Phys. **A 510** (1990) 1.